

Basic Filters for Convolutional Neural Networks Applied to Music: Training or Design?¹

M. Dörfler, T. Grill, R. Bammer, A. Flexer
monika.doerfler@univie.ac.at

Abstract: When convolutional neural networks are used to tackle learning problems based on music or, more generally, time series data, raw one-dimensional data are commonly pre-processed to obtain spectrogram or mel-spectrogram coefficients, which are then used as input to the actual neural network. In this contribution, we investigate, both theoretically and experimentally, the influence of this pre-processing step on the network's performance and pose the question, whether replacing it by applying adaptive or learned filters directly to the raw data, can improve learning success. The theoretical results show that approximately reproducing mel-spectrogram coefficients by applying adaptive filters and subsequent time-averaging is in principle possible. We also conducted extensive experimental work on the task of singing voice detection in music. The results of these experiments show that for classification based on Convolutional Neural Networks the features obtained from adaptive filter banks followed by time-averaging perform better than the canonical Fourier-transform-based mel-spectrogram coefficients. Alternative adaptive approaches with center frequencies or time-averaging lengths learned from training data perform equally well.

¹This work has been supported by the Vienna Science and Technology Fund (WWTF) through project MA14-018.

1 Introduction

Convolutional neural networks, first introduced in learning tasks for image data [18], have revolutionized state-of-the-art results in many machine learning (ML) problems. In convolutional neural networks (CNNs), when applied to image data, all filter coefficients are usually learned. For applications to time series, such as audio data, on the other hand, it is common practice to first apply a fixed filter bank to the raw, one-dimensional data in order to generate a feature representation. In traditional audio signal processing methods, used, e.g., in music information retrieval (MIR) or speech processing, FFT-based features such as *mel-spectrograms* are typically used as such inputs. These first level features are two-dimensional arrays, derived from some kind of windowed Fourier transform with subsequent mel-scale averaging.

Recently, the natural question arose, what kind of filters a network would learn if it was given the raw audio input. To date, encouraging results are scarce and so far, a true end-to-end approach for music signals, i.e., acting on raw audio without any pre-processing, has not been able to outperform models based on linear-frequency spectrogram or mel-spectrogram input [7]. It has been argued that these two ubiquitous representations automatically capture invariances which are of importance for *all* audio signals, in particular, a kind of translation invariance in time (guaranteed by introducing the non-linear magnitude operation) and a certain stability, introduced by the mel-averaging, to frequency shifts and time-warping (cp. [2]).

In this contribution, we give a formal description of the action of mel-scale averaging on spectrogram coefficients. We show that the resulting mel-spectrogram coefficients can indeed be mimicked by applying *frequency-adaptive* filters, however, *followed by time-averaging* of each filter's output. In order to obtain a close approximation to mel-spectrogram coefficients, the frequency adaptive filter bank's output signals must each undergo a time-averaging operation and the time-averaging window is different for each channel. Note that the similarity of mel-spectrogram coefficients to the result of time-averaging wavelet coefficients has already been observed in [2], without giving a precise formulation of the connection.²

We derive the necessary conditions on the filters, a different one for each bin in the mel-scale, by using the theory of Gabor multipliers and their spreading function, cf. [10]. Considering the description of an operator by means of its spreading function gives interesting insight in the nature of the correlations invoked by the application of the corresponding operator on the signal coefficients. In the case of mel-spectrogram coefficients it turns out that applying wide triangular windows in the high frequency regions actually corresponds to the application of an operator with little spreading in time. This seems to be the intuitively correct choice for audio signals such as music and speech. While a similar effect can be realized by applying wavelet or constant-Q type filters, the subsequent time-averaging alleviates the significant frequency-spreading effect introduced by rather narrow filtering windows. The observation gained from investigating the classical mel-spectrogram coefficients is thus, that time- and frequency-averaging

²This observation seems to have served as one motivation to introduce the so-called scattering transform, which consists of repeated composition of convolution, a nonlinearity in the form of taking the absolute value and time-averaging. In that framework, mel-spectrogram coefficients are interpreted as first order scattering coefficients.

spectrogram coefficients provide invariances which are useful in most audio classification tasks, cf. [3]. On the other hand, relaxing the strict averaging performed by computing mel-spectrogram coefficients may intuitively open the opportunity to keep information on details which may be necessary in certain learning tasks.

In our numerical experiments we thus strive to understand how time and frequency averaging influence CNN prediction performance on realistic data sets. The observations drawn from the experiments on learning filters can be summarized as follows:

- Using mel-spectrogram coefficients derived from convolutions with a small sub-sampling factor leads to improved results compared to the canonical FFT-based mel-spectrograms.
- Allowing the net to learn center frequencies or time-averaging lengths from the training data leads to comparable improved prediction results.
- Tricks are required to make the CNNs adapt the feature processing stage at all. Otherwise, the classification part of the network takes over the adaptation required to minimize the target loss.

This paper is organized as follows. In the next section we introduce necessary concepts from time-frequency analysis. In Section 3, we give a formal description of the network architecture, since we haven't found any concise exposition in the literature. Section 4 then gives the formal result linking mel-spectrogram coefficients with adaptive filterbanks. We also give a detailed analytical example based on Gaussian windows and present a numerical evaluation of the resulting approximation of mel-spectrogram coefficients. In Section 5 we report on the experiments with a real-world data set for the problem of singing voice detection. Finally we conclude with a discussion and perspectives in Section 6.

2 Time-frequency concepts

The Fourier transformation of a function $f \in \mathcal{H}$, for some Hilbertspace \mathcal{H} , will be denoted by $\mathcal{F}(f)$. We use the normalization $\mathcal{F}(f)(\omega) = \int_{\mathbb{R}} f(t)e^{2\pi i\omega t} dt$ and denote its inverse by $\mathcal{F}^{-1}(f)(t) = \int_{\mathbb{R}} f(\omega)e^{2\pi i\omega t} d\omega$. For $x, \omega \in \mathbb{R}$, the translation or time shift operator of a function f is defined as

$$T_x f(t) = f(t - x).$$

and the modulation or frequency shift operator of a function f is defined as

$$M_\omega f(t) = e^{2\pi i t \omega} f(t).$$

The operators of the form $T_x M_\omega$ or $M_\omega T_x$ are called time-frequency shifts. To obtain local information about the frequency spectrum we define the short-time Fourier transform (STFT) of a function f with respect to a window $g \neq 0$, where $f, g \in \mathcal{H}$, as

$$\mathcal{V}_g f(b, k) = \int_t f(t) \overline{g(t - b)} e^{-2\pi i k t} dt = \mathcal{F}(f \cdot T_b g)(k). \quad (1)$$

The STFT can be written as an inner product combining the above introduced operators

$$\mathcal{V}_g f(b, k) = \langle f, M_k T_b g \rangle.$$

Taking the absolute value squared we obtain the spectrogram as $S_0(b, k) = |\mathcal{V}_g f(b, k)|^2$ and $\mathcal{V}_g g$ is called ambiguity function of g , reflecting the time-frequency concentration of g . Note that in the definition given in (1), $\mathcal{V}_g f$ is a continuous function on \mathbb{R}^2 . In practice, subsampled and finite versions are used, cf. [8]. Sub-sampling obviously corresponds to choosing certain parts of the available information and this choice can have influence in particular for subsequent processing steps. This issue is further discussed in Section 3.2 and Section 4.

3 The structure of CNNs

The basic, modular structure of CNNs has often been described, see e.g., [13]. Here, we will give a formal statement of the specific architecture used in the experiments in this paper. This architecture has been successfully applied to several MIR tasks and seems to have a prototypical character for audio applications, cf. [14].

The most basic building block in a general neural network may be written as

$$x_{n+1} = \sigma(A_n x_n + b_n)$$

where x_n is the data vector, or array, in the n -th layer, A_n represents a linear operator, b_n is a vector of biases in the n -th layer and the nonlinearity σ is applied component-wise. Note that in each layer the array x_n may have a different dimension. Now, in the case of convolutional layers of CNNs, the matrix A has a particular structure for the convolutional layers, namely, it is a block-Toeplitz matrix, or, depending on the implementation of the filters, a concatenation of circular matrices, each representing one convolution kernel. There may be an arbitrarily high number of convolutional layers, followed by a certain number of so-called dense layers, for which A_n is again an arbitrary linear operator. In this paper, the chosen architecture comprises up to four convolutional and two or three dense layers.

REMARK 3.1. Note that it has been observed in [19, 22] that in the context of scattering networks, most of the input signal’s energy is contained in the output of the first two convolutional layers. While the context and the filters here are different, this observation might be interesting also as a background for the usual choice of architecture of CNNs for audio processing.

3.1 The CNN with spectrogram input

The standard input in learning methods for audio signal is based on a sub-sampled spectrogram, either in its raw form, or after some pre-processing such as the computation of mel-spectrogram, cf. Equation (4) in Section 4, which we will consider in detail in Section 4. In any case, the input to the CNN is a matrix of size $M \times N$.

REMARK 3.2. In most MIR tasks, the inputs are derived from rather short snippets, that is, about 2 to 4 seconds of sound. Considering a sampling rate of 22050 Hz, a window

size of 2048 samples and a time shift parameter of 512 samples, i.e., 23 ms, the resulting spectrogram (containing positive frequencies only) is of size $M \times N = 1024 \times 130$, where the latter is the time dimension. Hence, the frequency dimension is, in some sense, over-sampled. In particular, individual bins in the higher frequency regions contain less energy and thus information than in lower regions. Computing the mel-spectrogram is a convenient and straight-forward method of reducing the information to typically 80 frequency channels by averaging over increasingly many frequency bins.

We now define the following building blocks of a typical CNN:

- Convolution: $S * w(m, n) := \sum_{m'} \sum_{n'} S(m', n') w(m - m', n - n')$
- Pooling: For $1 \leq p \leq \infty$, we define $A \times B$ pooling as the operator mapping an $M \times N$ matrix S_0 to a $M/A \times N/B$ matrix S_1 by

$$S_1(m, n) = P_p^{A,B}(m, n) = \|v_{S_0}^{m,n}\|_p$$

where $v_{S_0}^{m,n}$ is the vector consisting of the matrix entries $S_0((m-1) \cdot A + 1, \dots, m \cdot A; (n-1) \cdot B + 1, \dots, n \cdot B)$ for $m = 1, \dots, M/A$, $n = 1, \dots, N/B$. In this work, we use max-pooling, which has been the most successful choice, corresponding to $p = \infty$ in the above formula.

- A nonlinearity $\sigma : \mathbb{R} \mapsto \mathbb{R}$, whose action is always to be understood component-wise. In all but the last layer we use leaky rectified linear units, which allow for a small, non-zero gradient when the unit is not active:

$$\sigma(x) = \begin{cases} x & \text{if } x > 0 \\ cx & \text{otherwise} \end{cases}$$

for some $c \ll 1$.

The output layer's nonlinearity σ_o is a sigmoid function. Given the above definitions, we can now write the output of a convolutional layer with an input array $S_n^{k_{n-1}} \in \mathbb{R}^{M_n \times N_n \times K_{n-1}}$:

$$S_{n+1}^{k_n} = \underbrace{P_\infty^{A_n, B_n} \sigma \left(\sum_{k_{n-1}=1}^{K_{n-1}} \underbrace{S_n^{k_{n-1}} * w_{k_n}^{k_{n-1}}}_{M_n \times N_n \times K_{n-1} \times K_n} + b^{k_n} \otimes \mathbf{1} \right)}_{M_n/A_n \times N_n/B_n \times K_n} \quad (2)$$

where $\mathbf{1}$ is an all-ones matrix of size $M_n \times N_n$, $b^{k_n} \in \mathbb{R}^{K_n}$ and $S_{n+1}^{k_n} \in \mathbb{R}^{M_n/A_n \times N_n/B_n}$ for $k_n = 1, \dots, K_n$. Letting D_c denote the number of convolutional layers and $S_{D_c}^{k_{D_c-1}} \in \mathbb{R}^{M_{D_c} \times N_{D_c} \times K_{D_c-1}}$ the output of the last convolutional layer, the over-all action of a CNN with two dense layers, and considering, for simplicity, a single output unit emitting x_{out} , can be written as

$$x_{out} = \sigma_o(\mathcal{A}_2 \cdot [\sigma(\mathcal{A}_1 \cdot S_{D_c}^{k_{D_c-1}} + b^{D_c+1})] + b^{D_c+2}) \quad (3)$$

Here, \mathcal{A}_1 and \mathcal{A}_2 are weight-matrices of size $N_d \times M_{D_c} N_{D_c} K_{D_c-1}$ and $1 \times N_d$, respectively, where N_d is the number of hidden units in the first dense layer, $b^{D_c+1} \in \mathbb{R}^{N_d}$ and $b^{D_c+2} \in \mathbb{R}$.

3.2 Modifying the input matrix

As mentioned in the previous section, the spectrogram of audio is often pre-processed in order to reduce the dimensionality on the one hand, and in order to obtain a spectral representation that better fits both human perception and properties of speech and music on the other hand. Additionally, the authors in [2] pointed out that using mel-spectrogram instead of the spectrogram guarantees improved stability with respect to frequency shifts or, more generally, deformations of the original audio signals, than the usage of spectrograms. However, *given appropriate choice of network architecture*, comparable results can usually be achieved using either the spectrogram or the mel-spectrogram, i.e., the invariance introduced by the mel-averaging can also be learned. In other respects, omitting the frequency-averaging provided by the mel-spectrogram leads to an increase in the number of weights to be learned. On the other hand, this observation raises the question, whether using filters learned directly in the time-domain, would improve the net’s ability to achieve the amount of invariance most appropriate for a particular ML task and thus increase stability. The corresponding approach then implies learning time-domain filters already in a layer prior to the first 2D-convolution. To put this remark into perspective, we note that the spectrogram may easily be interpreted as the combined (and possibly sub-sampled) output of several convolutions, since, setting $\check{h}(n) = h(-n)$, we can write

$$S_0(m, n) = \left| \sum_{n'} f(n') h(n' - n) e^{-2\pi i m n'} \right|^2 = |f * \check{h}_m(n)|^2$$

3.3 Questions

In the two following sections we thus raise and answer two questions:

- (i) Is it possible to obtain coefficients which are approximately equivalent to the well-established mel-spectrogram coefficients simply by using the ‘correct’ filters directly on the audio signal?
- (ii) Can adaptivity in frequency- and time-averaging improve prediction accuracy? In particular, for a given set of frequency-adaptive filters precisely mimicking the mel-scale, can a time-averaging layer with learned averaging width improve learning performance?

4 The mel-spectrogram and basic filters

In this section, we take a detailed look at the mel-spectrogram. This representation is derived from the classical spectrogram by weighted averaging of the absolute values squared of the STFT and can undoubtedly be referred to as the most important feature set used in speech and audio processing, together with MFCCs which are directly derived from it. The number of mel-filters used varies between 80 filters between 80 Hz and 16 kHz [14] and 128 [7] or more. In order to better understand the relation between the result of mel-averaging and FFT-based analysis with flexible windows, we observe the following: denote the input signal by $f \in \mathbb{C}^N$, the window function for generating the spectrogram by $g \in \mathbb{C}^N$ and the mel-filters, typically given by simple triangular functions,

by $\Lambda_\nu \in \mathbb{C}^N$ for $\nu = 1 \dots K$, where K is the chosen number of filters. We can then write the mel-spectrogram as

$$\text{MS}_g(f)(b, \nu) = \sum_k |\mathcal{F}(f \cdot T_b g)(k)|^2 \cdot \Lambda_\nu(k). \quad (4)$$

Andén and Mallat showed in [2], that the mel-spectrogram can be approximated by time-averaging the absolute values squared of a wavelet transform. Here, we make their considerations precise by showing that we can get a close approximation of the mel-spectrogram coefficients if we use adaptive filters.

REMARK 4.1. Note that the resulting transform may be interpreted as a nonstationary Gabor transform, compare [5, 4, 16, 9].

Proposition 4.2. *Let an analysis window g and mel-filters Λ_ν be given, for $\nu \in \mathcal{I}$. If, for each ν , the windows h_ν and time-averaging functions ϖ_ν are chosen such that*

$$V_{h_\nu} h_\nu(x, \xi) \cdot \mathcal{F}(\varpi_\nu)(\xi) = V_g g(x, \xi) \cdot \mathcal{F}^{-1}(\Lambda_\nu)(x), \quad (5)$$

then the mel-spectrogram coefficients $\text{MS}_g(f)(b, \nu)$ can be obtained by time-averaging the filtered signal's absolute value squared as follows:

$$\text{MS}_g(f)(b, \nu) = \sum_l |(f * h_\nu)(l)|^2 \cdot \varpi_\nu(l - b) =: \text{TA}^h(f)(b, \nu). \quad (6)$$

The proof is given in Appendix A.

While it is in general tedious to derive conditions for the optimal filters h_ν and the time-averaging windows ϖ_ν explicitly, we obtain a more accessible situation if we restrict the choice of windows to dilated Gaussians. In this case we set $g(t) = \varphi_\sigma(t) = (\frac{2}{\sigma})^{\frac{1}{4}} e^{-\pi \frac{t^2}{\sigma}}$. Then we have, by straight-forward computation,

$$\mathcal{V}_{\varphi_\sigma} \varphi_\sigma(x, \xi) = e^{-\frac{\pi}{2} \frac{x^2}{\sigma}} e^{-\frac{\pi}{2} \sigma \xi^2} e^{-\pi i x \xi},$$

which leads to the following result:

Corollary 4.3. *Fix $g = \varphi_\sigma$ for some scaling factor σ , and let the filters Λ_ν be given as shifted and possibly dilated versions of a basic shape (e.g., in the case of mel-filters, asymmetric triangular functions), i.e., $\Lambda_\nu(\xi) = T_\nu D_{a(\nu)} \Lambda(\xi)$, for $\nu \in \mathcal{I}$.*

Assuming that each filter h_ν is a Gaussian window $\varphi_{\rho(\nu)}$ with a frequency-dependent dilation factor $\rho(\nu)$ and frequency-shifted to position ν , i.e., $h_\nu(t) = e^{2\pi i \nu t} \varphi_{\rho(\nu)}(t)$. Then condition (5) is equivalent to the following conditions in separate variables:

$$e^{-\frac{\pi}{2} x^2 (\frac{1}{\rho(\nu)} - \frac{1}{\sigma})} = \mathcal{F}^{-1}(D_{a(\nu)} \Lambda)(x) \quad (7)$$

$$e^{-\frac{\pi}{2} \xi^2 (\sigma - \rho(\nu))} = \mathcal{F}(\varpi_\nu)(\xi). \quad (8)$$

Proof: Noting that $V_{h_\nu} h_\nu(x, \xi) = e^{2\pi i \nu x} V_{\varphi_{\rho(\nu)}} \varphi_{\rho(\nu)}(x, \xi)$ and that $\mathcal{F}^{-1}(\Lambda_\nu)(x) = e^{2\pi i \nu x} \mathcal{F}^{-1}(D_{a(\nu)} \Lambda)(x)$, the result is straight-forward. ■

REMARK 4.4. From the above corollary we see that a precise recovery of the mel-spectrogram coefficients by means of time-averaging of the spectrogram coefficients with respect to any dilated Gaussian window is only possible if the averaging windows $D_{a(\nu)}\Lambda$ are themselves dilated Gaussians. However, we may deduce the following pointwise error estimate:

$$|\text{MS}_g(f)(b, \nu) - \text{TA}^h(f)(b, \nu)| \leq \|V_{h_\nu} h_\nu \cdot \mathcal{F}(\varpi_\nu) - V_g g \cdot \mathcal{F}^{-1}(\Lambda_\nu)\|_2 \quad (9)$$

Even if the mel-spectrogram coefficients can not precisely be recovered by adaptive filtering followed by time-averaging, a close approximation can be achieved for reasonable windows g . However, excellent precision of approximation is only achieved in the case of full spectrograms, i.e., if no subsampling is applied and declines with increasingly coarse subsampling strategies. The sub-sampled case leads to aliases, as stated in the next corollary.

Corollary 4.5. *If, for given g, h_ν and Λ, ϖ_ν , the mel-spectrogram coefficients (4) and the time-averaging coefficients (6) are computed using time- and frequency subsampling by α and β , respectively, then the approximation error is bounded by*

$$|\text{MS}_g^{\alpha, \beta}(f)(b, \nu) - \text{TA}^{\alpha, \beta, h}(f)(b, \nu)| \leq \|V_{h_\nu} h_\nu \sum_k T_{\frac{k}{\alpha}} \mathcal{F}(\varpi_\nu) - V_g g \sum_l T_{\frac{l}{\beta}} \mathcal{F}^{-1}(\Lambda_\nu)\|_2 \cdot \|f\|_2^2 \quad (10)$$

A technical proof of Corollary 4.5 is included in Appendix A. Intuitively it is clear that, if the time- and frequency variable in (1) are sub-sampled by α and β , respectively, $\mathcal{F}(\varpi_\nu)$ and $\mathcal{F}^{-1}(\Lambda_\nu)$ are periodic with period $\frac{1}{\alpha}$ and $\frac{1}{\beta}$. The aliases showing up in the error bound (10) deteriorate the approximation of the mel-coefficients. In the realistic scenarios addressed in Section 5, which always involve subsampled spectrograms, the differences between mel-spectrogram coefficients and their approximation by adaptive filtering become relevant for the performance of CNN-learning. However, we may indeed obtain a less biased estimate, in comparison to the mel-spectrogram coefficients, of the frequencies present in a certain time segment of a signal by increasing the sampling density α , which corresponds to *decreasing* the convolution stride. On the other hand, the frequency sampling density β is implicitly defined by the windows' length in samples and the corresponding FFT-length, which may also be increased.

4.1 Computation and examples of adaptive filters

In this section, we give some examples of filters h_ν computed to obtain mel-coefficients $\text{MS}_g(f)$ by time-averaging $|(f * h_\nu)(l)|^2$ as in (6). We consider Hann windows, which is the standard choice in audio processing, also applied in the computation of mel-spectrogram coefficients and their approximation in Section 5. Starting from a Hann window g , we compute adaptive filters h_ν for 80 bins of the mel-scale. Since the ambiguity function $\mathcal{V}_g g(x, \xi)$ of a Hann window does not exactly factorize in independent components in each of the variables x, ξ , we use the following trick for computing h_ν for a given mel-filter Λ_ν : we consider the right-hand side of (5) in $\xi = 0$. This is justified by the observation that $\mathcal{F}(g)$, and thus $\mathcal{V}_g g$, decays fast in the frequency variable ξ . We then have, with $\check{g}(x) = \bar{g}(-x)$:

$$V_g g(x, 0) \cdot \mathcal{F}^{-1}(\Lambda_\nu)(x) = (g * \check{g})(x) \cdot \mathcal{F}^{-1}(\Lambda_\nu)(x)$$

and, applying the same consideration to the left-hand side of (5) and taking Fourier transform:

$$\mathcal{F}(h_\nu * \check{h}_\nu) = |\mathcal{F}(h_\nu)(\xi)|^2 = \mathcal{F}((g * \check{g}) \cdot \mathcal{F}^{-1}(\Lambda_\nu))(\xi),$$

so that we obtain h_ν as

$$h_\nu(t) = \mathcal{F}^{-1} \left(\sqrt{\mathcal{F}((g * \check{g}) \cdot \mathcal{F}^{-1}(\Lambda_\nu))} \right) (t)$$

Similarly, by setting $x = 0$ in the left-hand side of (5), we compute

$$\mathcal{F}(\varpi_\nu)(\xi) = V_g g(0, \xi) \cdot \mathcal{F}^{-1}(\Lambda_\nu)(0) / V_{h_\nu} h_\nu(0, \xi)$$

where we only consider values of $V_{h_\nu} h_\nu(0, \xi)$ above a threshold ε .

Figure 1 shows the ambiguity functions $V_g g$, $V_{h_\nu} h_\nu$, and the weighted ambiguity functions $V_g g \cdot \mathcal{F}^{-1}(\Lambda_\nu)$, $V_{h_\nu} h_\nu \cdot \mathcal{F}(\varpi_\nu)(\xi)$, for $\nu = 49$, which corresponds to 2587.6 Hz.

In Figure 2, the upper plot shows the original Hann and three adapted windows, narrowing with increasing mel-number to realize the mel-averaging by adaptivity in the frequency domain. The lower plot shows the average error per bin obtained from computing the mel-spectrogram coefficients and their approximations for 200 (normally distributed) random signals.

For an illustration of the time-frequency representations applied to a real audio signal, cf. Figure 3.

5 Experiments on Singing Voice Detection

In Proposition 4.2 it is shown that coefficients with mel-characteristics (and other related nonlinear scales) can be closely approximated by applying appropriately chosen filters directly to raw audio data and allowing for a subsequent time-averaging step. Now, we are interested in investigating if the theoretical findings translate to typical real-world problems that have already been successfully treated with CNNs. Thereby, we are motivated by the fact that state-of-the-art results for several MIR problems are based on mel-spectrogram coefficients which show certain desirable invariance and stability properties. In particular, due to the modulus, they are invariant to translation and, due to the frequency averaging, they exhibit stability to certain deformations such as time-warping, cf. [2]. However, in general, the required invariance and stability with respect to deformations will depend on data characteristics and the learning task, cf. [20]. Hence, we start from our construction encompassing adaptive filtering followed by time-averaging. Alternatively, we allow parts of the feature processing stage (time-averaging lengths, center frequencies) to be learned by the network, posing the question whether adaptivity in this step can improve the network’s performance.

We need to note that, when trained on a specific problem, both the feature layers (including the adaptive time-averaging step) and the classification part of a CNN will concurrently adapt their parameters towards optimally predicting the given targets. We will discuss the implications of this behavior for our experiments in Section 5.4.

Our hypothesis is that a CNN with an architecture that is adapted to a given learning task will learn filters — in this case their adaptive components — which alleviate the extraction of stabilities and invariance properties and are thus beneficial in the given context.

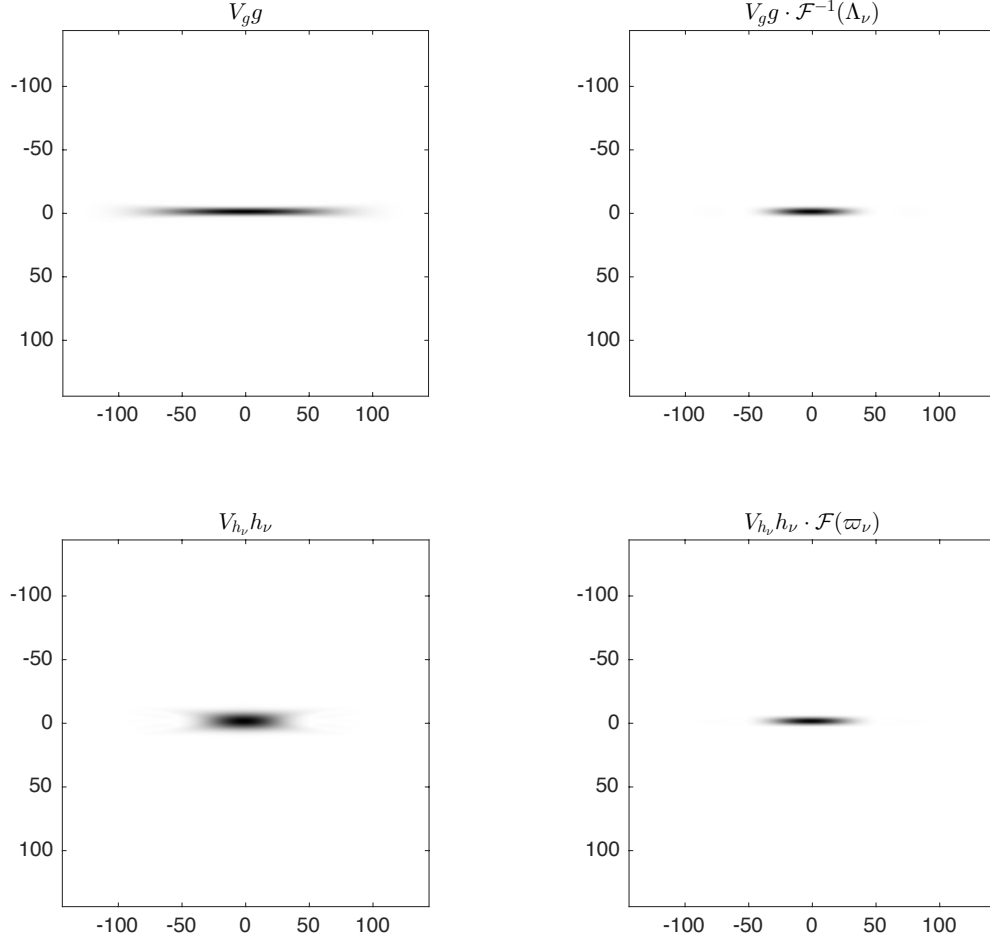


Figure 1: Ambiguity functions $V_g g$, $V_{h_\nu} h_\nu$, and weighted ambiguity functions $V_g g \cdot \mathcal{F}^{-1}(\Lambda_\nu)$, $V_{h_\nu} h_\nu \cdot \mathcal{F}(\varpi_\nu)(\xi)$ used for the computation of adaptive filtering, for $\nu = 50$. It is clearly visible that the surplus in frequency spread introduced by the narrower window h_ν is removed by time-averaging. On the other hand, frequency averaging reduces the time-spread of the wider window g .

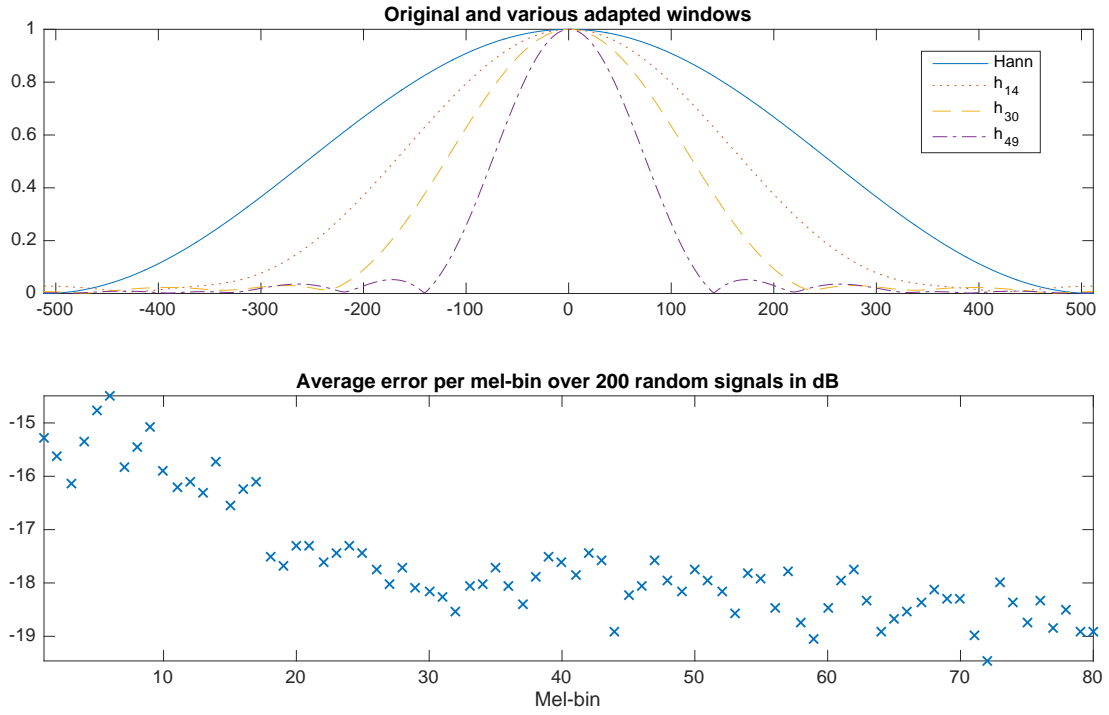


Figure 2: Upper plot: (original) Hann window and adapted windows; lower plot: error in approximation of mel-spectrogram coefficients by adaptive filtering and subsequent time-averaging

5.1 Data

We investigate the effects of learning filters directly on raw audio by revisiting the problem of *singing voice detection* [21] we have studied before. In the referenced publication, a CNN was tuned for maximum prediction accuracy both in the absence or presence of various forms of data augmentation.

The experiments were performed on a non-public dataset of 188 30-second audio snippets from an online music store (dataset ‘In-House A’), covering a very wide range of genres and origins. We used a five-fold cross-validation, for each iteration 150 files for training, the remaining 38 for evaluation. The audio was subsampled to a sampling rate of 22.05 kHz and down-mixed to mono. The mel-spectrograms were calculated using an STFT with Hann windows, a frame length of 1024 and a frame rate of 70 per second (equivalent to a hop size of 315 samples).

For this paper, instead of magnitude spectra, as in the reference model, we use power spectra as in Equation 4, also following the convention used in [2]. We apply a filter-bank with 80 triangular mel-scaled filters from 27.5 Hz to 8 kHz, then logarithmize the squared magnitudes (after clipping values below 10^{-7}).

5.2 CNN training procedure and architecture

The training procedure used in our experiments is slightly different than in the reference publication [21]. The networks are trained on mel-spectrogram excerpts of 115 spectrogram frames (~ 1.6 seconds) paired with a label denoting the presence or absence of human voice in the central frame. Training is performed using stochastic gradient descent on cross-entropy error based on mini-batches of 64 randomly chosen examples. Updates to the network weights are computed using the ADAM update rule [17] with an initial learning rate of 0.001 and an adaptive scheme reducing the learning rate twice by a factor of 10 whenever the training error does not improve over three consecutive episodes of 1000 updates. Evaluation is performed running a complete five-fold cross-validation run to obtain predictions for the whole set of training data, with this procedure repeated multiple times with different network initialization and data ordering.

As described in Section 3.1, the applied CNN architecture employs three types of feed-forward neural network layers: convolutional *feature processing layers* convolving a stack of 2D inputs with a set of learned 2D kernels, *pooling layers* subsampling a stack of 2D inputs by taking the maximum over small groups of neighboring pixels, and dense *classification layers* flattening the input to a vector and applying a dot product with a learned weight matrix \mathcal{A}_j .

The architecture used in [21] has a total number of 1.41 million weights, with the dense connections of the classification layers taking up the major share (1.28 million, or 91%). It can be expected that the actual output of the convolutional feature stage is of subordinate importance when the classification stage with its high explanatory power dominates the network.

If data augmentation is not considered, the network size — especially the classification part — can be drastically reduced while largely preserving its performance. This size reduction is possible, since, as a general rule, the necessary number of parameters determining the network is correspondent to the complexity of the training data set. As we are interested in the impact of the convolutional feature stage’s properties, we reduce

the architecture for our experiments as follows: We use four convolutional layers, two 3×3 convolutions of 32 and 16 kernels, respectively, followed by 3×3 non-overlapping max-pooling and two more 3×3 convolutions of 32 and 16 kernels, respectively, and another 3×3 pooling stage.

In the notation of (2), this corresponds to

- $K_0 = K_2 = 32, K_1 = K_3 = 16$
- $w_{k_0} \in \mathbb{R}^{3 \times 3}, k_0 = 1, \dots, 32;$
- $w_{k_1}^{k_0} \in \mathbb{R}^{3 \times 3 \times 32}, k_1 = 1, \dots, 16$
- $A_1 = B_1 = 1, A_2 = B_2 = 3$
- $w_{k_2}^{k_1} \in \mathbb{R}^{3 \times 3 \times 16}, k_2 = 1, \dots, 32;$
- $w_{k_3}^{k_2} \in \mathbb{R}^{3 \times 3 \times 32}, k_3 = 1, \dots, 16$
- $A_3 = B_3 = 1, A_4 = B_4 = 3$

For the classification part, we experimented with two variants: One with two dense layers of 64 and 16 units (‘small-two’), and the other one with just one dense layer of 32 units (‘small-one’). In both cases, the final dense layer is a single sigmoidal output unit. For the first variant, the total number of weights is 94337, with the classification stage taking up 79969 units, or 85%. The second variant features a considerably smaller classification network: the total number of weights is 53857, with the classification stage taking up 39489 units, or 73%. The different network sizes, especially the ratio of feature to classification stage allows us to analyze the influence of the different parts. Specifically, we expect the performance of the ‘small-one’ architecture to be more directly connected to the quality of the time-frequency representation.

5.3 Experimental setup

In the following, we will compare the behavior of the CNNs applied to the STFT-based mel-spectrogram features to features computed using filter banks as described in Section 4. Both are computed in end-to-end fashion ad hoc from the audio signal. The maximum kernel sizes of the filter banks are set to 1024, identical to the frame length of the previously used STFT. The training examples are snippets of the audio signal with a length of $115 \times 315 + 1024 - 1 = 37248$ samples each with a hop size of 315 samples.

To judge the influence of adaptivity, four different approaches have been compared:

1. ‘Filterbank, approximation’: Filter bank and time averaging as derived in Section 4
2. ‘Filterbank, naive’: Filter bank with Hann envelopes. The kernel size equals the time support for the lowest frequency band (50 Hz) and reduces, according to the band-width requirements of the mel frequency scale, down to 94 samples for the highest band at 7740 Hz. After the filter bank, fixed-size time-averaging by pooling for improved computational efficiency.
3. ‘Filterbank, fixed-width’: Filter bank as in 2., but with fixed-size time-averaging using a convolution with a Hann window

4. ‘Filterbank, variable-width’: Adaptive time-averaging after the filter bank, with individual adaptation per frequency bin, learned from the training data.

For reasons of computational cost it is not feasible to perform a full sample-by-sample convolution for the filter bank. For the bulk of our filter-bank experiments, we have chosen a convolution stride for the filters of 21 samples, that is, the resulting spectrum is down-sampled along the time axis by a factor of 21. The subsequent non-overlapping averaging is computed on 15 frames each, in order to stay comparable with the STFT hop size of $315 = 21 \times 15$ samples. Note that the stride is a factor of about 4.5 lower than the shortest kernel support (21 vs. 94). For comparison, we have also experimented with smaller convolution strides to assess their impact on the results.

For the ‘naive’ fixed-size time-averaging variant standard average-pooling is used, implemented as a 15×1 2D-pooling layer acting on the power spectrum. In this case the temporal averaging length is uniform over the frequency axis which is a crude approximation of the mathematical findings. The ‘fixed-width’ and ‘variable-width’ cases are implemented using Hann windows, the latter with adaptive width, individual for each frequency bin. The maximum time support of this Hann window is 8 times the STFT hop size, equivalent to 2520 samples. The choice of Hann in contrast to a Boxcar window (as in the ‘naive’ case) is motivated by its smoothness which enables adaptivity for the CNN training process.

Figure 3 illustrates the time-frequency representations used in this paper. The STFT case is shown on the left-hand-side with the full Fourier spectrum (512 bins) on top and its mel-spectrogram (80 bins) at the bottom. On the right-hand-side, the top shows a filter-bank-computed mel-scaled spectrogram using the filters derived in Section 4, and the time-averaged counterpart at the bottom. Note that the two bottom spectrograms are equivalent.

5.4 Experimental results

Figure 4 shows the results of our CNN experiments for the problem of singing voice detection. For our evaluations, we have switched from the simple error measure with the ‘optimal’ (in the sense of maximum accuracy) threshold per experiment to the more informative ‘area over the ROC curve’ measure (AOC), fusing classification errors for all possible thresholds into one measure. A lower measure indicates a better result.

The reference implementation in [21] uses pre-computed spectrograms, with a normalization globally on the the training set and eventual padding performed also on the spectrogram. End-to-end learning as performed in our experiments demands on-line normalization (using a batch normalization layer) and padding directly on the audio time signal. We could verify that this yields a performance equivalent with the reference experiments.

We can also confirm that the performance of our ‘small-two’ network with two classification layers is comparable to the large baseline architecture. For AOC (STFT case), the smaller networks score 6.66% (‘small-two’) and 7.05% (‘small-one’), respectively, compared to 6.82% of the original architecture (not shown in the figure). The difference between the reference and the ‘small-two’ architecture is not significant (t-test, $p = 5\%$), while the difference between ‘small-two’ and ‘small-one’ is.

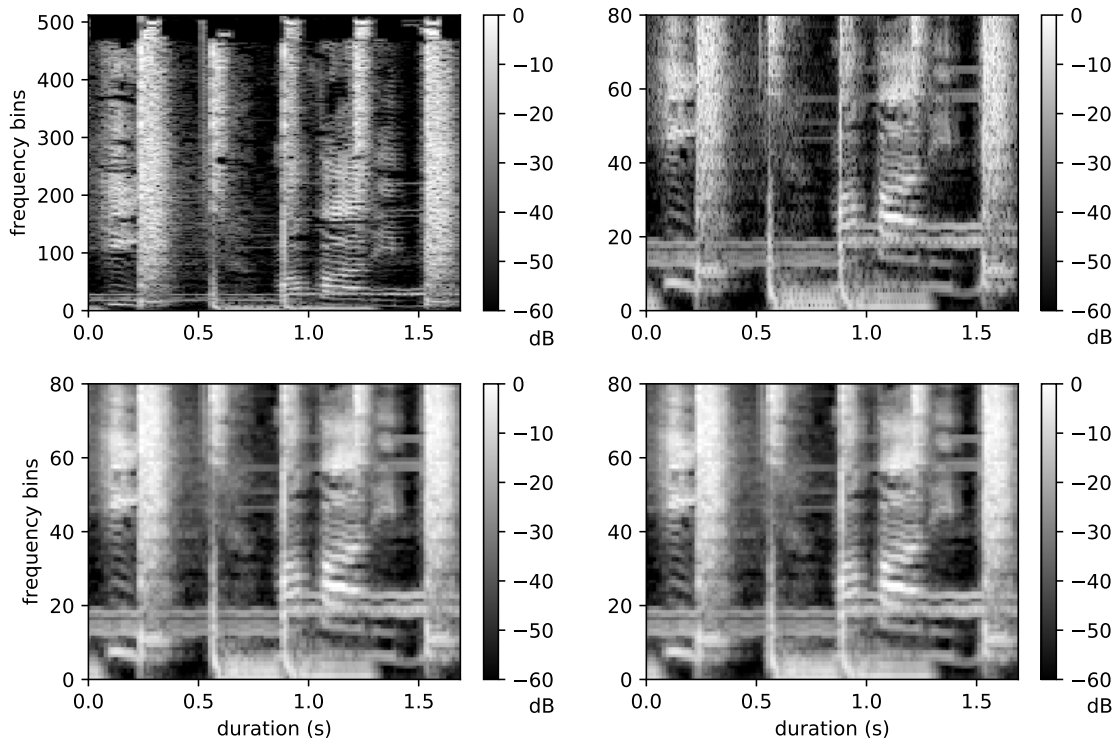


Figure 3: Time-frequency representations for the problem of singing voice detection. The spectrograms shown are STFT (upper left), STFT-based mel spectrogram (bottom left), filter-bank computed (top right), and filter-bank with time-averaging (bottom right).

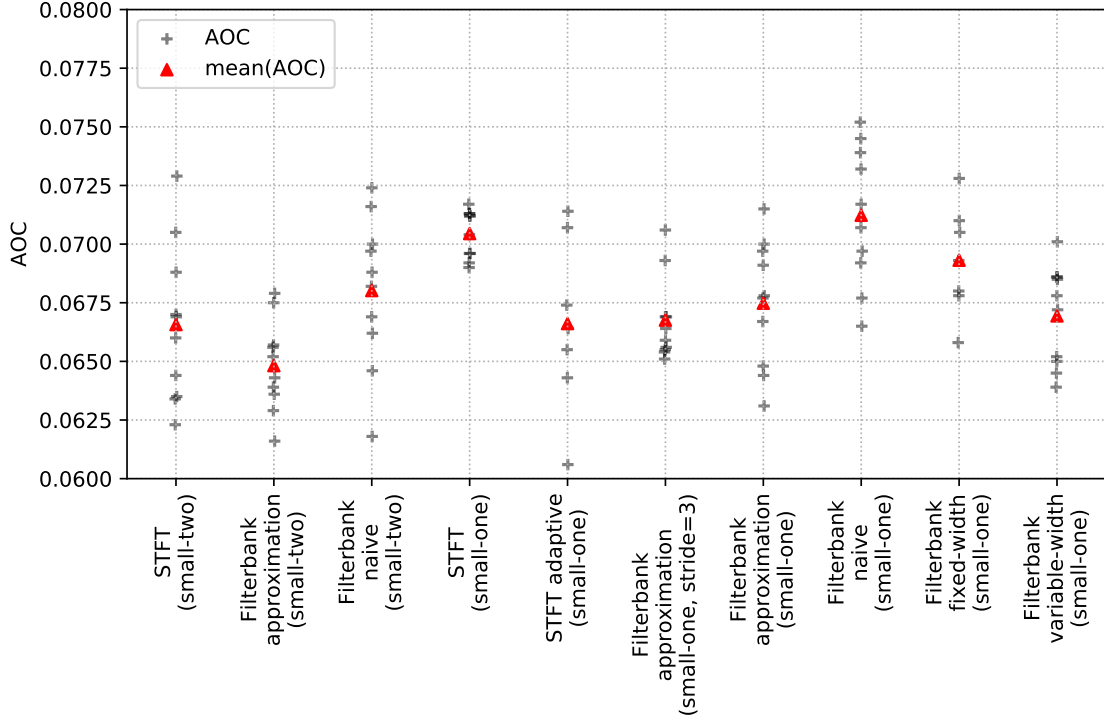


Figure 4: AOC measures for the problem of singing voice detection. Models compared are results for multiple runs of five-fold cross-validation on batch-normalized mel-spectrograms (*STFT*), on batch-normalized Filter banks with fixed-width temporal averaging (*Filterbank naive*), with the approximative filters derived in Section 4 (*Filterbank approximation*), and with adaptive variable-width averaging (*Filterbank variable-width*), for both CNN architectures ‘small-two’ and ‘small-one’. Shown are individual results (gray crosses), mean (red triangles) and median (green dots) values.

In the course of experimentation it has become apparent that the time-averaging widths of the adaptive models hardly train at all, especially for larger classification stages. They rather stay close to the initial values, while the CNN weights adapt instead. As a trick we have *boosted* the widths’ gradients for the back-propagation by a factor 3 to force the width parameters to adapt at a higher rate. Higher factors have proven unfeasible, causing the adaptation to run out of bounds. Since the adaptation process is intricate, the choice of a starting value for the variable averaging length (time support of the Hann window) is important. We have tried values of 0.1, 0.2, 0.3, 0.5 of the maximum time support, with 0.2 (equivalent to 504 samples) leading to the best results.

For both architectures, we see in Figure 4 that the filter-bank approximation scores better than the canonical STFT case (significant for the ‘small-one’ architecture at $p < 5\%$) which can be explained by the impact of frequency-aliases which are described in the error bound in (10): using a convolution stride of 21 corresponds to a subsampling factor $\alpha = 21/1024 = 0.02$ in time as opposed to $\alpha = 315/1024 = 0.3$ in the STFT case. Heuristically, we obtain a more stable estimate for the local frequency components, cp. the recent work in [1]. We were able to confirm this trend by using even smaller convolution strides (subsampling factor 3 instead of the standard 21) which led to a slightly, albeit insignificantly, better score. These observations indicate that the actual time-frequency resolution of the signal representation used in the first processing step can lead to advantages in the over-all performance of the CNN, which cannot necessarily be provided by subsequent convolutional or dense layers. To our knowledge, this is the first formal description of such an effect.

In comparison to the filter-banks with filter coefficient approximations according to the theory, the ‘naive’ (significant at $p = 5\%$) and the ‘fixed-width’ (not significant) variations exhibit slightly worse performance for both architectures. The ‘variable-width’ variation with adaptive time-averaging scores significantly better than its ‘fixed-width’ counterpart, and is statistically equivalent ($p > 60\%$) to the filter-bank ‘approximation’ case.

At the same level of performance lies the ‘STFT adaptive’ case which is a variation of the STFT case with adaptive (learned in CNN training) center frequencies for the triangular filter-bank applied to the Fourier frequency spectrum.

In general, and as expected, the effects of adaptivity on the evaluation results are more pronounced for the smaller architecture, with less explanatory power in the classification stages.

6 Discussion and perspectives

In Section 3.3 we posed two questions concerning the application of alternative time-frequency representations for learning problems in music information retrieval.

First, it has been analytically shown under which conditions mel-spectrogram coefficients can be reproduced by applying frequency-adaptive filters followed by a time-averaging step. In practice, this procedure will always lead to approximate values due to their computation from sub-sampled values.

Answering the second question, we have found that these *designed* spectrogram representations yield significantly increased performance on the task of CNN-based singing

voice detection. The improvement in performance can be ascribed to a sub-sampling scheme implicit in the usage of the designed adaptive filters, which yields a more advantageous suppression of adversarial time-frequency aliases than the canonical computation of mel-spectrogram coefficients. Furthermore, adaptivity by *training* in the time-averaging layer, or alternatively, using frequency-adaptive triangular filters on the Fourier spectrograms, on the other hand, also lead to improved results relative to the canonical STFT-based mel-spectrograms. These results are performance-wise statistically equivalent to the filters derived by the mathematical theory developed in Section 4. Hence, similar results were obtained both with properly *designed* representations and representations whose crucial parameters were *trained* on the data.

Summing up, we conclude that the subtle differences in time-frequency resolution of the basic filters used to obtain the signal representation do influence the over-all performance of a CNN applied to a typical MIR task, at least for architectures of rather modest size.

Future work on the problem of learned basic filters in MIR tasks will involve the study of the precise connection between the characteristics of a given data set and the most advantageous analysis windows and sampling schemes used to compute the spectrogram. These investigations will concern both the network’s expressivity and the performance of the learning process, cf. preliminary work in [9] and will be based on data sets with different time-frequency characteristics as well as various learning tasks. Finally, future work will also address the more general question of the propagation and alleviation of small approximation errors through the network and their dependence on various network parameters as well as the network’s architecture, relying on existing results on stability of CNNs, compare [23, 6, 15].

A Invariance properties induced by filters: Technical details

A.1 Proof of Proposition 4.2 and Corollary 4.5

In order to include the situation described in Corollary 4.5, we assume the situation in which the original spectrogram is sub-sampled, in other words, we start the computations concerning a signal f from

$$S_0(\alpha l, \beta k) = |\mathcal{V}_g f(\alpha l, \beta k)|^2 = |\mathcal{F}(f \cdot T_{\alpha l} g)(\beta k)|^2.$$

The proof of Proposition 4.2 is based on the observation that the mel-spectrogram can be written via the operation of so-called *STFT- or Gabor-multipliers*, cf. [12], on any given function in the sense of a bilinear form. Before deriving the involved correspondence, we thus introduce this important class of operators.

Given a window function g , time- and frequency-sub-sampling parameters α, β , respectively, and a function $\mathbf{m} : \mathbb{Z} \times \mathbb{Z} \mapsto \mathbb{C}$, the corresponding Gabor multiplier $G_{g_\alpha^\beta, \mathbf{m}}$ is defined as

$$G_{g_\alpha^\beta, \mathbf{m}} f = \sum_k \sum_l \mathbf{m}(k, l) \langle f, M_{k\beta} T_{l\alpha} g \rangle M_{k\beta} T_{l\alpha} g.$$

We next derive the expression of a mel-spectrogram by an appropriately chosen Gabor multiplier. Using sub-sampling factors α in time and β in frequency as before, we start

from (4) and reformulate as follows:

$$\begin{aligned}
\text{MS}_g(f)(b, \nu) &= \sum_k |\mathcal{F}(f \cdot T_b g)(\beta k)|^2 \cdot \Lambda_\nu(k) \\
&= \sum_k \langle f, M_{\beta k} T_b g \rangle \overline{\langle f, M_{\beta k} T_b g \rangle} \Lambda_\nu(k) \\
&= \left\langle \sum_k \Lambda_\nu(k) \langle f, M_{\beta k} T_b g \rangle M_{\beta k} T_b g, f \right\rangle \\
&= \left\langle \sum_k \sum_l \mathbf{m}(k, l) \langle f, M_{\beta k} T_{\alpha l} g \rangle M_{\beta k} T_{\alpha l} g, f \right\rangle
\end{aligned}$$

with $\mathbf{m}(k, l) = \delta(\alpha l - b) \Lambda_\nu(k)$. We see that the mel-coefficients can thus be interpreted via a Gabor multiplier: $\text{MS}_g(f)(b, \nu) = \langle G_{g_{\alpha, \mathbf{m}}^\beta} f, f \rangle$.

The next step is to switch to an alternative operator representation. Indeed, as shown in [11], every operator H can equally be written by means of its *spreading function* η_H as

$$Hf(t) = \int_x \int_\xi \eta_H(x, \xi) f(t - x) e^{2\pi i t \xi} d\xi dx. \quad (11)$$

We note that two operators H_1, H_2 are equal if and only if their spreading functions coincide, see [10, 11] for details.

As shown in [10], a Gabor multiplier's spreading function $\eta_{g_{\alpha, \mathbf{m}}^\beta}$ is given by

$$\eta_{g_{\alpha, \mathbf{m}}^\beta}(x, \xi) = \mathcal{M}(x, \xi) \mathcal{V}_g g(x, \xi), \quad (12)$$

where $\mathcal{M}(x, \xi)$ denotes the $(\beta^{-1}, \alpha^{-1})$ -periodic symplectic Fourier transform of \mathbf{m} , i.e.,

$$\mathcal{M}(x, \xi) = \mathcal{F}_s(\mathbf{m})(x, \xi) = \sum_k \sum_l \mathbf{m}(k, l) e^{-2\pi i (l \alpha \xi - k \beta x)}. \quad (13)$$

We now equally rewrite the time-averaging operation applied to a filtered signal, as defined in (6), as a Gabor multiplier. As before, we set $\check{h}_\nu(t) = \overline{h_\nu(-t)}$ and have

$$\begin{aligned}
&\sum_l |(f * h_\nu)(\alpha l)|^2 \cdot \varpi_\nu(\alpha l - b) = \sum_l \left| \sum_n f(n) \check{h}_\nu(n - \alpha l) \right|^2 \cdot \varpi_\nu(\alpha l - b) \\
&= \sum_k \sum_l |\langle f, M_{\beta k} T_{\alpha l} \check{h}_\nu \rangle|^2 \cdot \varpi_\nu(\alpha l - b) \delta(k) = \langle G_{\check{h}_{\alpha \nu}^\beta, \mathbf{m}_T} f, f \rangle.
\end{aligned}$$

with $\mathbf{m}_T(k, l) = T_b \varpi_\nu(l) \delta(k)$.

In order to compare the two operators $G_{g_{\alpha, \mathbf{m}}^\beta}$ and $G_{\check{h}_{\alpha \nu}^\beta, \mathbf{m}_T}$, we compute their respective spreading functions; we apply the symplectic Fourier transform (13) to $\mathbf{m} = T_b \delta \cdot \Lambda_\nu$ and $\mathbf{m}_T = T_b \varpi_\nu \cdot \delta$ to find:

$$\mathcal{M}(x, \xi) = \mathcal{F}_s(\mathbf{m})(x, \xi) = e^{-2\pi i b \xi} \cdot \mathcal{F}^{-1}(\Lambda_\nu)(x)$$

and

$$\mathcal{M}_T(x, \xi) = \mathcal{F}_s(\mathbf{m}_T)(x, \xi) = e^{-2\pi i b \xi} \cdot \mathcal{F}(\varpi_\nu)(\xi)$$

Plugging these expressions into (12) yields the condition in Proposition 4.2 and thus concludes its proof.

To obtain the error estimate in Corollary 4.5, first note that, by straight-forward computation using the operators' representation by their spreading functions as in (11)

$$\begin{aligned} |\text{MS}_g^{\alpha,\beta}(f)(b, \nu) - \text{TA}^{\alpha,\beta,h}(f)(b, \nu)| &= | \langle (G_{g_\alpha, \mathbf{m}}^\beta - G_{h_{\alpha\nu}, \mathbf{m}_T}^\beta) f, f \rangle | \\ &= | \langle (\eta_{g_\alpha, \mathbf{m}}^\beta - \eta_{h_{\alpha\nu}, \mathbf{m}_T}^\beta), \mathcal{V}_f f \rangle | \leq \| \eta_{g_\alpha, \mathbf{m}}^\beta - \eta_{h_{\alpha\nu}, \mathbf{m}_T}^\beta \| \cdot \| f \|_2^2 \end{aligned}$$

and we can estimate the error by the difference of the spreading functions. In order to quantify the impact of sub-sampling, we write the sampled version of Λ_ν by using the Dirac comb III_β : $\Lambda_\nu(\beta k) = (\text{III}_\beta \Lambda_\nu)(t) = \sum_k \Lambda_\nu(t) \delta(t - k\beta)$ and analogously for ϖ_ν by applying III_α . Now it is a well-known fact that the Fourier transform turns sampling with sampling interval β into periodisation by $1/\beta$, in other words, into a convolution with $\text{III}_{\frac{1}{\beta}}$. Therefore, for Λ_ν sampled on $\beta\mathbb{Z}$:

$$\mathcal{F}^{-1}(\text{III}_\beta \Lambda_\nu)(x) = \text{III}_{\frac{1}{\beta}} * \mathcal{F}^{-1}(\Lambda_\nu)(x) = \sum_l T_{\frac{l}{\beta}} \mathcal{F}^{-1}(\Lambda_\nu)(x).$$

Completely analogous considerations for ϖ_ν and III_α lead to the periodization of $\mathcal{F}(\varpi_\nu)$ and thus the bound given in (10).

REMARK A.1. It is interesting to interpret the action of an operator in terms of its spreading function. In view of (11), we see that the spreading function determines the amount of shift in time and frequency, which the action of the operator imposes on a function. For Gabor multipliers, if well-concentrated window functions are used, it is immediately obvious that the amount of shifting is moderate as well as determined by the window's eccentricity. At the same time, the aliasing effects introduced by coarse sub-sampling are reflected in the periodic nature of \mathcal{M} . Since, for $\mathcal{F}^{-1}(\Lambda_\nu)$ the sub-sampling density in frequency, determined by β , and for $\mathcal{F}(\varpi_\nu)$ the sub-sampling density in time, determined by α , determine the amount of aliasing, the over-all approximation quality deteriorates with increasing sub-sampling factors.

References

- [1] Abreu, L., Romero, J.: Mse estimates for multitaper spectral estimation and off-grid compressive sensing. *IEEE Trans. Inf. Theory*. **63**(12), 7770 – 7776 (2017)
- [2] Andén, J., Mallat, S.: Deep scattering spectrum. *IEEE Transactions on Signal Processing* **62**(16), 4114–4128 (2014)
- [3] Anselmi, F., Leibo, J.Z., Rosasco, L., Mutch, J., Tacchetti, A., Poggio, T.A.: Un-supervised learning of invariant representations in hierarchical architectures. *CoRR abs/1311.4158* (2013). URL <http://arxiv.org/abs/1311.4158>
- [4] Balazs, P., Doerfler, M., Kowalski, M., Torresani, B.: Adapted and adaptive linear time-frequency representations: a synthesis point of view. *IEEE Signal Processing Magazine* **30**(6), 20–31 (2013)
- [5] Balazs, P., Dörfler, M., Jaillet, F., Holighaus, N., Velasco, G.: Theory, implementation and applications of nonstationary gabor frames. *Journal of computational and applied mathematics* **236**(6), 1481–1496 (2011)

- [6] Bammer, R., Dörfler, M.: Invariance and stability of gabor scattering for music signals. In: Sampling Theory and Applications (SampTA), 2017 International Conference on, pp. 299–302. IEEE (2017)
- [7] Dieleman, S., Schrauwen, B.: End-to-end learning for music audio. In: Acoustics, Speech and Signal Processing (ICASSP), 2014 IEEE International Conference on, pp. 6964–6968 (2014). DOI 10.1109/ICASSP.2014.6854950
- [8] Dörfler, M.: Time-frequency analysis for music signals: A mathematical approach. *Journal of New Music Research* **30**(1), 3–12 (2001)
- [9] Dörfler, M., Bammer, R., Grill, T.: Inside the spectrogram: Convolutional neural networks in audio processing. In: International Conference on Sampling Theory and Applications (SampTA), pp. 152–155. IEEE (2017)
- [10] Dörfler, M., Torrésani, B.: Representation of operators in the time-frequency domain and generalized Gabor multipliers. *J. Fourier Anal. Appl.* **16**(2), 261–293 (2010)
- [11] Feichtinger, H.G., Kozek, W.: Quantization of TF lattice-invariant operators on elementary LCA groups. In: H.G. Feichtinger, T. Strohmer (eds.) *Gabor analysis and algorithms*, Appl. Numer. Harmon. Anal., pp. 233–266. Birkhäuser Boston (1998)
- [12] Feichtinger, H.G., Nowak, K.: A first survey of Gabor multipliers. In: H.G. Feichtinger, T. Strohmer (eds.) *Advances in Gabor Analysis*, Appl. Numer. Harmon. Anal., pp. 99–128. Birkhäuser (2003)
- [13] Goodfellow, I., Bengio, Y., Courville, A.: *Deep learning*. MIT press (2016)
- [14] Grill, T., Schlüter, J.: Music Boundary Detection Using Neural Networks on Combined Features and Two-Level Annotations. In: *Proceedings of the 16th International Society for Music Information Retrieval Conference (ISMIR 2015)*. Malaga, Spain (2015)
- [15] Grohs, P., Wiatowski, T., Bölcskei, H.: Deep convolutional neural networks on cartoon functions. In: *Information Theory (ISIT), 2016 IEEE International Symposium on*, pp. 1163–1167. IEEE (2016)
- [16] Holighaus, N., Dörfler, M., Velasco, G.A., Grill, T.: A framework for invertible, real-time constant-Q transforms. *IEEE Trans. Audio Speech Lang. Process.* **21**(4), 775–785 (2013)
- [17] Kingma, D., Ba, J.: Adam: A method for stochastic optimization. In: *Proceedings of the 6th International Conference on Learning Representations (ICLR)*. San Diego, USA (2015)
- [18] LeCun, Y., Bottou, L., Bengio, Y., Haffner, P.: Gradient-based learning applied to document recognition. *Proceedings of the IEEE* **86**(11), 2278–2324 (1998)
- [19] Mallat, S.: Group Invariant Scattering. *Comm. Pure Appl. Math.* **65**(10), 1331–1398 (2012)

- [20] Mallat, S.: Understanding deep convolutional networks. *Philosophical Transactions of the Royal Society of London A: Mathematical, Physical and Engineering Sciences* **374**(2065) (2016). DOI 10.1098/rsta.2015.0203. URL <http://rsta.royalsocietypublishing.org/content/374/2065/20150203>
- [21] Schlüter, J., Grill, T.: Exploring Data Augmentation for Improved Singing Voice Detection with Neural Networks. In: *Proceedings of the 16th International Society for Music Information Retrieval Conference (ISMIR 2015)*. Malaga, Spain (2015)
- [22] Wiatowski, T., Grohs, P., Bölcskei, H.: Energy propagation in deep convolutional neural networks. *arXiv preprint arXiv:1704.03636* (2017)
- [23] Wiatowski, T., Tschannen, M., Stanic, A., Grohs, P., Bölcskei, H.: Discrete deep feature extraction: A theory and new architectures. In: *Proceedings of the International Conference on Machine Learning*, pp. 2149–2158 (2016)